That's how the preform crumples

Wrinkle creation during forming of thick binder-stabilised stacks of non-crimp fabrics

Broberg, Peter H.; Lindgaard, Esben; Krogh, Christian; Thompson, Adam J.; Belnoue, Jonathan P.H.; Hallett, Stephen R.; Bak, Brian L.V.

Published in:
Composites Part B: Engineering

DOI (link to publication from Publisher):
10.1016/j.compositesb.2024.111269

Publication date:
2024

Document Version
Publisher's PDF, also known as Version of record

Composites Part B 273 (2024) 111269

Contents lists available at ScienceDirect

Composites Part B

journal homepage: www.elsevier.com/locate/composites

That's how the preform crumples: Wrinkle creation during forming of thick binder-stabilised stacks of non-crimp fabrics

Peter H. Broberg [a,*], Esben Lindgaard [a], Christian Krogh [a], Adam J. Thompson [b], Jonathan P.-H. Belnoue [b], Stephen R. Hallett [b], Brian L.V. Bak [a]

[a] CraCS Research Group (cracs.aau.dk), Department of Materials and Production, Aalborg University, Fibigerstræde 16, DK-9220, Aalborg East, Denmark
[b] Bristol Composite Institute, University of Bristol, Queens Building, BS8 1TR, Bristol, UK

ARTICLE INFO

Keywords:
A. Preform
B. Defects
E. Forming
Process modelling
Wrinkles
Non-crimp fabrics

ABSTRACT

The simultaneous forming of multiple layers of fabric is being used in industry to increase the throughput of composite parts. A polymeric binder may be used to stabilise the fabric layers to make it easier to handle, however, the binder may also restrict relative fibre movement, which may lead to wrinkles during forming. Despite the increasing interest in using binder-stabilised preforms in the wind industry, defects arising during forming have scarcely been investigated. This study investigates fibre wrinkling in binder-stabilised preforms (layers of dry non-crimp fabric stabilised with an interply polymeric binder) during forming. The results from an experimental campaign are presented, in which full-thickness pre-consolidated preform specimens are being formed over two different ramp geometries. Wrinkles are observed at the transition edges during forming. To aid the discussion on wrinkle mechanisms, a numerical model is presented that uses continuum shell elements for modelling the NCFs and a cohesive law for modelling the interface. This model is capable of predicting the wrinkle onset and wrinkle location and may be used to study the formability of the preform.

1. Introduction

Fibre-reinforced composite materials are becoming the first choice in a wide array of applications ranging from sports equipment to large off-shore wind turbine blades. The size of wind turbine blades has increased rapidly during the last decade to increase the wind turbine power output [1]. Current blades exceed 100 metres, and the dimensions are expected to further increase in the future [2]. Wind turbine blades are, typically, manufactured using Vacuum Assisted Resin Transfer Moulding (VARTM), in which dry non-crimp fabric and inserts are placed in a one-sided mould prior to resin infusion. Conventional manufacturing of wind turbine blades relies mostly on manual handling of individual fabric plies, which makes manufacturing of large blades slow. However, the use of binder-stabilised preforms has recently received attention in the industry to enable increased throughput and automation of blade production [3]. Binder-stabilised preforms are stacks of dry fabric with a polymeric binder in between the individual layers to stabilise the preform and ensure easy handling [4]. By using binder stabilisation, the critical main blade mould cycle time can be reduced by using different tools for preforming and moulding. This also helps minimise undesired fibre movement as the preforming tools are simpler, and the binder fixates the fabrics. During the last decades, the use of binder-stabilised preforms in combination with resin transfer moulding (RTM) has seen several advances in other industries, such as the automotive industry [5], to obtain fast processing of composite parts while suppressing manufacturing defects [6]. However, a far greater amount of reinforcement material is needed in wind turbine blades, which may lead to new mechanisms for defect generation. Knowledge of the defects arising during the manufacturing of thick binder-stabilised preforms is, therefore, needed to transfer the preform technology to blade production.

One of the most significant manufacturing defects in fibre composites is fibre wrinkling (fibre waviness) [7], which is known to severely decrease the load-carrying capabilities of the finished cured composite structure [8–10]. In [10] a knock-down in the strength of over 60% has been reported for some wrinkle configurations in wind turbine blades. Wrinkles may arise during all steps involved in the manufacturing of composite structures [11], but the present investigation focuses on wrinkles arising during forming of dry reinforcement. Early literature regards the *shear locking angle* (the in-plane shear angle at which the resistance to further shearing increases) as the main wrinkling mechanism [12]. More recently, the bending stiffness of the fabric and

* Corresponding author.
E-mail addresses: phb@mp.aau.dk (P.H. Broberg), elo@mp.aau.dk (E. Lindgaard), ck@mp.aau.dk (C. Krogh), adam.thompson@bristol.ac.uk (A.J. Thompson), jonathan.belnoue@bristol.ac.uk (J.P.-H. Belnoue), stephen.hallett@bristol.ac.uk (S.R. Hallett), brianbak@mp.aau.dk (B.L.V. Bak).

https://doi.org/10.1016/j.compositesb.2024.111269
Received 4 September 2023; Received in revised form 12 January 2024; Accepted 30 January 2024
Available online 1 February 2024

process parameters have been shown to significantly influence wrinkle creation [13,14]. During the simultaneous forming of multiple fabrics, the interface between the separate fabric layers has a large impact on wrinkle creation [15]. The main mechanism leading to wrinkles during forming is inter-ply friction impeding the ply slippage [16–20]. In [21] the lay-up sequence was also shown to have a significant effect on out-of-plane wrinkling, whereas ply thickness and fibre friction may contribute to large wrinkling through coupling effects. Currently, most studies on wrinkle mechanisms during the forming of multiple fabric layers are on prepreg systems or non-bindered dry fabrics. To the authors' knowledge, no description of binder properties on wrinkle creation has been reported in the literature. Even though the use of binder material on dry fabric preforms increases the dimensional stability [22], it also impedes fibre slippage, which may lead to out-of-plane wrinkling at transitions in the mould [23].

Composite process models may be used to predict manufacturing defects, which can greatly reduce the cost related to expensive trial and error experiments in industry. The simulation models can, generally, be divided into kinematical and mechanical models. The kinematic models rely on strong assumptions on the fabric behaviour and are mostly used for draping analysis of a single ply on a mould [24]. The kinematic models are computationally efficient but do not take the complex material behaviour and manufacturing process into account. Mechanical models often use finite element analysis and are suitable for studying wrinkle creation [14]. In process simulations, the fabric material is typically modelled on the macro-scale by considering the fabric as a homogenous continuum [25]. In these models, the bending and membrane stiffness are often decoupled to account for specific fabric behaviour associated with relative fibre movement on the micro-scale. Several ways of decoupling the bending and membrane stiffness have been explored in literature including using an asymmetric bending stiffness [26], superimposing shell and membrane elements [27,28], using a fictive 3-layer laminate layup [29,30], and making user-defined elements [14].

When stacks of fabrics are formed over an external radius on the tool, wrinkling may occur due to the relative arc length of the plies changing during forming. A similar mechanism occurs when stacks of fabrics are consolidated over a radius on the mould/tool [31]. Therefore, simulation models for predicting wrinkles during forming and consolidation will both be covered here. Some models for predicting wrinkles during the simultaneous forming of multiple fabrics have considered frictional laws in the interface [19,32]. In some forming models for prepreg materials, tack between individual plies has been described with a cohesive law in normal direction [33,34]. Process models for predicting defects during consolidation additionally include compaction behaviour to the material models [35–37]. Similar finite element models have been used to study the creasing and folding of cardboard material describing the cardboard interface with a cohesive law [38]. In other literature, a thick interlock reinforcement has been modelled as a 3D continuum [39]. This modelling approach is efficient for thick composite parts, however, it cannot consider delamination of the binder and wrinkle creation through the thickness.

Current studies on the wrinkle creation during forming of multi-layered preforms primarily focus on prepreg materials [21] or biaxial NCFs [40]. To the authors' knowledge, no study has previously investigated fibre wrinkling arising during forming of thick binder-stabilised stacks of UD-NCF. The aim of this paper is to investigate the mechanisms leading to wrinkles in binder-stabilised preforms through an experimental forming trial over a geometric transition. In addition, a new preform-forming model will be proposed to aid the discussion on the wrinkle mechanisms.

The rest of the paper is structured as follows: in Section 2, the experimental campaign for investigating wrinkle creation in binder stabilised preforms is presented. This includes a description of the experimental setup and a presentation of the results. To aid the discussion on wrinkle mechanisms, a numerical model is presented in Section 3 with the results from simulating the forming of the preforms. In Section 4 the mechanisms leading to wrinkles in binder-stabilised preforms are discussed. Finally, the paper is concluded in Section 5.

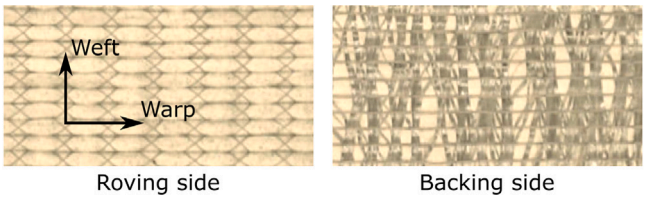

Fig. 1. Image of the UD-NCF used in the preform.

2. Experiments

2.1. Description of the preform test specimens

The preform considered in this study consists of 16 layers of glass fibre non-crimp fabric (NCF) with an area weight of 1380 g/m^2. Each layer consists of 96 wt% H-glass fibres with a fibre diameter of 17 to 24 micrometres oriented at 0°. There are 4 wt% E-glass backing fibres with a fibre diameter of 9 micrometres oriented at ±80°. The fibre angles are given relative to the warp direction of the fabric, see Fig. 1. The stitch is a combined tricot-chain stitch of polyester thread. The thickness of a single layer is approximately 1 mm. The preform is consolidated at elevated temperatures using a soluble polyester binder with 15 g/m^2 dispersed on the roving side of the fabric in powder form. The binder primarily bonds the backing fibres to the rovings of the adjacent fibre mat. The total thickness of the preform specimens is approximately 16 mm. After consolidation, the preform is cut into test specimens with dimensions 1000 mm × 50 mm × 16 mm (Length × Width × Thickness). The length is measured along the UD-fibre direction and the thickness is measured in the stacking direction. Transverse normals are painted on the side of the preform specimen every 20 mm along the length of the specimen. These are used to measure the transverse shearing of the preform during loading.

2.2. Description of the benchmark case

Forming of pre-consolidated preform specimens over a mould with a ramp geometry is considered in the present study, see Fig. 2. The ramp geometry is very common in wind turbine blades, e.g. at core material transitions and tapered inserts at the root section [9,10]. The preform technology for wind turbine blades is still being developed. The closer the preform geometry is to the final geometry, the more expensive the manufacturing is due to more complicated tooling and higher requirements for placement tolerances. For this study, the simplest, and thus the least expensive from a manufacturing point of view, preform geometry is chosen.

When an initially straight fibre preform is formed over a ramp, wrinkles may arise at the transition edges due to a relative change in the arc length of the plies. Fibre wrinkling occurs when there is an excess of fibre material, which may happen if the preform does not shear sufficiently, see Fig. 2. Please note that the shearing referred to here is the transverse shearing of the preform and not the in-plane intra-ply shearing commonly associated with fibre wrinkling. The transverse shearing of the preform occurs due to a combination of inter-ply sliding and transverse intra-ply shearing [41]. If the amount of preform shearing is equal to the angle of the ramp, no wrinkles are anticipated, as this entails that there will be no excess of material at the transition edges.

In this study, two different ramp geometries are considered. The dimensions of the two benchmark geometries are listed in Table 1. Benchmark 2 is representative of material transitions in wind turbine blades, while benchmark 1 has an aggressive taper angle for enhancing effects occurring during forming.

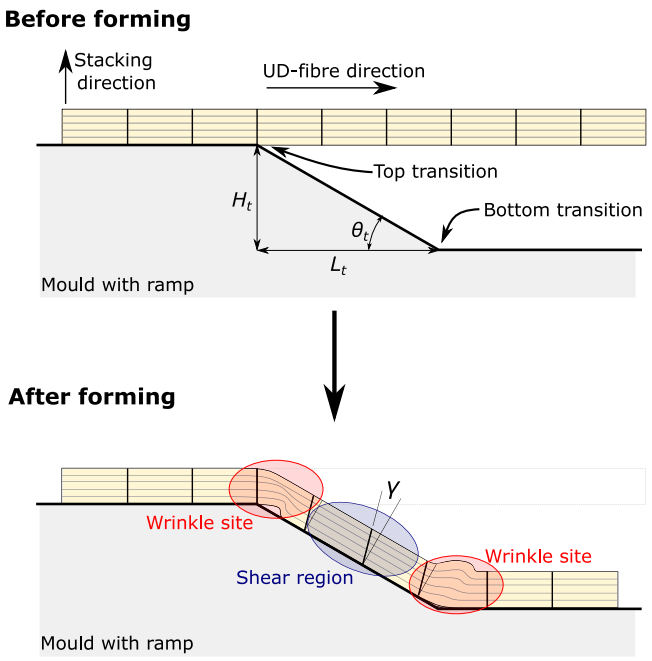

Fig. 2. Forming of a preform over a ramp geometry.

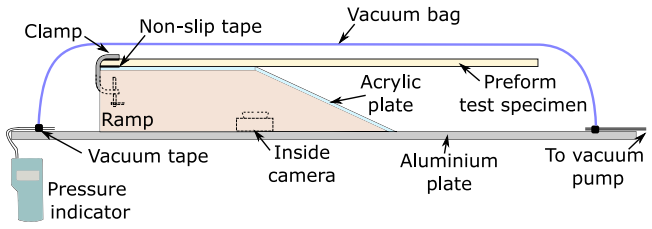

Fig. 3. Experimental setup.

Table 1
Dimensions of the two ramp benchmark geometries considered.

	L_t	H_t	θ_t
Benchmark 1	320 mm	150 mm	25.1°
Benchmark 2	600 mm	60 mm	5.7°

2.3. Experimental methodology

The experiments are carried out by forming the preform specimens over the ramp geometry by applying a vacuum on the specimen. A sketch of the experimental setup is shown in Fig. 3. The preform specimens are placed on a ramp with the dimensions listed in Table 1. The ramp is made of MDF plates with acrylic plates on top. The ramp is hollow, and the acrylic plates allow for a camera to be placed inside the ramp to record the preform during forming. In this way, the camera may observe wrinkles not visible from the surface. A vacuum bag is placed over the specimen and ramp, and the vacuum is applied by a vacuum pump. A *GE Druck DPI705* is used to gauge the vacuum pressure. The preform specimen is fixed to the ramp by a steel clamp with a smooth surface to avoid puncture to the vacuum bag during loading. A small strip of non-slip tape is applied on both the clamp and acrylic plate to avoid slippage of the preform during forming.

Five tests are carried out on each of the benchmark geometries, using new specimens for each repeat. Each specimen is loaded until 50% vacuum. The vacuum is applied in the course of 30 s. After 50% vacuum is reached, the pressure is maintained while images are taken

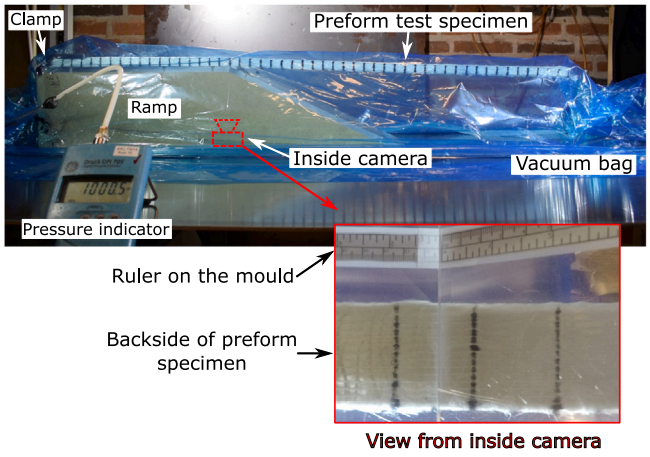

Fig. 4. Image of the experimental setup prior to vacuum being applied.

and the location and the size of the wrinkles are measured. Two *NILA Zaila Daylight* cool LED white light sources are used to illuminate the preform specimen and a camera is used to film the forming process. An image of the setup from the camera and an image from the inside camera is shown in Fig. 4. The experiments are carried out at room temperature.

2.4. Experimental results

Representative images from the experiments are shown in Fig. 5. Two types of wrinkles are observed in the experiments: small wrinkles and large wrinkles (see Fig. 5). The small wrinkles (or roving-buckling) are wrinkling of the UD-rovings between the stitches. The small wrinkles have a length equal to the distance between the stitches. Large wrinkles (or ply buckling) are wrinkling of the whole NCF ply. The length of the large wrinkles typically spans multiple stitches. The large wrinkles can be either located on the bag side (surface wrinkles) or the mould side (mould wrinkles). Small wrinkles are only observed on the bag side (external surface), as small mould wrinkles cannot be detected by the inside camera. The wrinkle pattern for all the tests carried out on geometry 1 was very similar and is sketched in Fig. 6. The large wrinkles are measured and quantified by their location, P, length, L, and amplitude, A, see Fig. 6. In tests 2, 3, and 5 on geometry 1 two large wrinkles are observed at the bottom transition. The smallest of the two wrinkles at the bottom transition in tests 2, 3, and 5 is termed *2nd wrinkle at the bottom transition*. The transverse shear angle of the preform, γ, is measured in the shear region (Fig. 2). On geometry 2, no large wrinkles were observed in any of the five tests carried out, however, the transverse shear angle in the shear region was still measured.

The average wrinkle metrics and transverse shear angles with standard deviations for the five tests of the experiment on geometry 1 (steep ramp) are listed in Table 2. The maximum value, minimum value, and coefficient of variation (CoV) for the wrinkle metrics are included in the table. The coefficient of variation is not included for the wrinkle placement as this value depends on the zero point. In each of the five tests, a large mould wrinkle is observed at the top transition. The location of the wrinkle at the top transition varies between −11 mm (relative to the top transition) and 0 mm. The large mould wrinkles are not visible from the surface of the top layer. At the bottom transition, large surface wrinkles are observed in all tests for geometry 1. The location of the 1st wrinkle at the bottom transition varies between −23 mm (relative to the bottom transition) and 60 mm. This variation is greater than for the mould wrinkle at the top transition. This may be due to the uncertainties and variations in how the load is applied and variability in the specimens. Furthermore, in some of the tests, small surface wrinkles

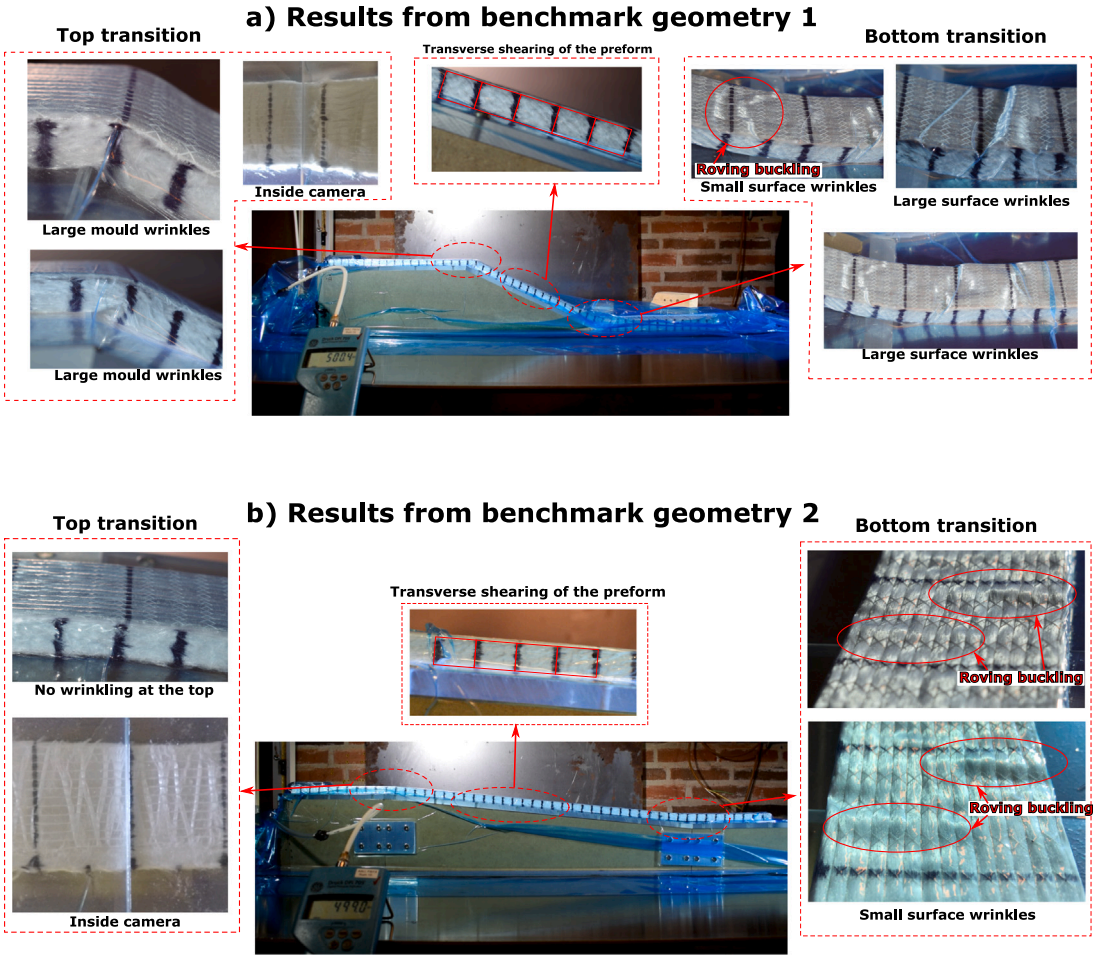

Fig. 5. Representative images from the experiments. For the specimens formed over geometry 1, large wrinkles are observed at the top and bottom transition, (a), while small wrinkles are observed in the specimens formed over geometry 2, (b).

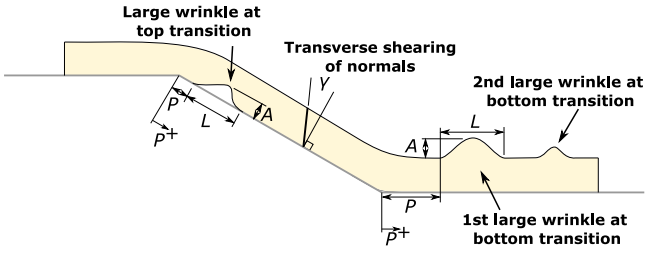

Fig. 6. Naming convention and metrics for the wrinkles and transverse shear angle. The 2nd large wrinkle at the bottom transition is measured similarly to the 1st large wrinkle.

(roving-buckling) are observed at the bottom transition. These small wrinkles may also be present at the top transition, however, they cannot be detected since the backing side is facing the camera placed inside the ramp. The average transverse shear angle of the preform specimens was measured to 7.1°. The angle of the geometry is 25.1°, which means that there is a difference of 18° between the transverse shear angle and the ramp angle. By assuming that the preform deforms in simple shear and the fibres are inextensible, this amount of shear difference causes an excessive fibre length of $\Delta S = t \times \tan(\Delta\theta)$, where t is the thickness of the preform and $\Delta\theta$ is the difference between the transverse shear angle and the angle of the ramp. This results in an excessive fibre length of $\Delta S = 5.2$ mm at each transition, which may cause the observed fibre wrinkling.

Table 2
Results from the experimental forming on geometry 1.

Large wrinkle at the top transition					
	Avg ± SD	Min	Max	CoV	FE-sim
P	−2.8 ± 4.3 mm	−11 mm	0 mm	–	−17 mm
L	13 ± 4.3 mm	8 mm	21 mm	33%	30 mm
A	3.5 ± 1.1 mm	2 mm	5 mm	31%	12 mm
1st large wrinkle at the bottom transition					
	Avg ± SD	Min	Max	CoV	FE-sim
P	+29 ± 28 mm	−23 mm	+60 mm	–	−2 mm
L	37 ± 8.6 mm	26 mm	50 mm	23%	54 mm
A	4.6 ± 1.4 mm	3 mm	7 mm	30%	11 mm
2nd large wrinkle at the bottom transition (test 2, 3, and 5)					
	Avg ± SD	Min	Max	CoV	FE-sim
P	+57 ± 48 mm	−10 mm	+100 mm	–	–
L	13 ± 4.7 mm	10 mm	20 mm	36%	–
A	2.3 ± 0.5 mm	2 mm	3 mm	22%	–
Transverse shear angle					
	Avg ± SD	Min	Max	CoV	FE-sim
γ	7.1° ± 1.0°	5.3°	8.2°	14%	4.5°

In geometry 2, no large wrinkles are observed at the transition edges in all the tests carried out, see Fig. 5. There are, however, small surface wrinkles observed at the bottom transition for all five tests, but none at the top transition. The average, min and max transverse shear angle for the test on geometry 2 are listed in Table 3. The average transverse shear angle is 1.9° and the ramp has an angle of 5.7°, which means

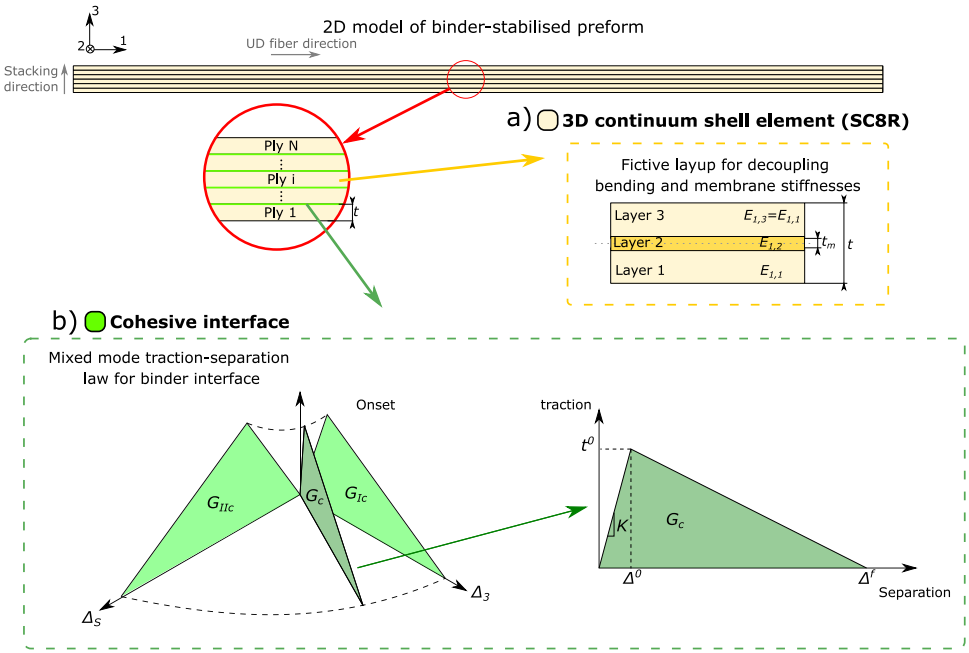

Fig. 7. Sketch of the numerical model. (a) The NCFs are modelled using continuum shell elements (SC8R in ABAQUS) with a fictive 3-layer laminate layup for decoupling the bending and membrane stiffness. (b) The binder is modelled as a cohesive interface with a mixed-mode traction-separation law.

Table 3
Results from the experimental forming on geometry 2.

	Transverse shear angle				
	Avg ± SD	Min	Max	CoV	FE-sim
γ	1.9° ± 0.2°	1.7°	2.2°	11%	2.5°

that there is a difference of 3.8° and an excessive fibre length of 1 mm at each transition.

The total height of the preforms is measured to 15.5 mm during loading on both geometry 1 and 2. This means that the preforms have compacted with 0.5 mm due to the vacuum pressure. The excessive fabric length at a convex transition due to the compaction can be estimated kinematically with $\Delta S_{\text{compaction}} = S_{\text{before}} - S_{\text{after}}$ [35]. S_{before} is the arc length of the top layer of fabric at the transition before compaction, which is given by $S_{\text{before}} = (R + t) \times \theta_t$, where R is the transition radius, θ_t is the transition angle, and t is the initial preform thickness. S_{after} is the arc length of the top layer of fabric after compaction, which is given by $S_{\text{after}} = (R + t_c) \times \theta_t$, where t_c is the compacted thickness. Inserting the expressions for the fabric length before and after compaction results in an excessive fabric length of $\Delta S = (t - t_c) \times \theta_t$ due to compaction. This results in an excessive length of $\Delta S = 0.25$ mm on geometry 1 and $\Delta S = 0.05$ mm on geometry 2. The compaction-induced effects are, thus, much smaller than the forming-induced effects.

3. Modelling

3.1. Numerical model

To help understand the mechanisms leading to the wrinkles observed in the experimental program, a numerical model is developed. The model is made using conventional approaches for modelling fabrics and weak interfaces. Similar modelling approaches have previously been shown to represent wrinkle creation in preforms [42]. These methods are adapted to the preform material considered and can be used to study strain distribution and damage degradation associated with wrinkle creation. The numerical model was run in ABAQUS using an explicit finite element analysis. The preform is modelled on a macro-scale, which means that the NCF plies are considered as a homogenous continuum and the binder interface is modelled as a homogenous interface. This macro-scale model allows for computationally efficient solutions while still providing information on the inter-ply mechanisms and ply wrinkling. A schematic of the model is shown in Fig. 7. The NCF plies are modelled using 3D continuum shell elements (SC8R). 3D continuum shell elements are used instead of shell elements as they improve the contact formulation between the NCFs by describing the interface with a well-defined geometry [43]. In this study, the stiffness in the stacking direction (E_3) does not influence the critical time step as a reasonably fine discretisation of the elements is used ($L_e = 0.005$ m) to represent the wrinkling. The element discretisation is chosen based on a mesh convergence study. Further refinement of the model yields similar wrinkling behaviour. The location of the wrinkle at the bottom transition is slightly sensitive to changes in mesh size. This results from the wrinkle at the bottom transition generally being more sensitive to small variations, which is also evident from the experimental results. To decouple the bending and the membrane stiffness of each NCF ply, each layer is represented by a single SC8R element through the thickness with a 3-layer fictive laminate layup [29]. The fictive laminate layup is chosen as it is directly applicable with the continuum shell elements. The fictive layup, as illustrated in Fig. 7, consists of two different layer stiffnesses. $E_{1,1}$ for layer 1 and 3, and $E_{1,2}$ for layer 2 and given by:

$$E_{1,1} = \frac{3D_{11} - E_1 t_m^2 t/4}{t^3/8 - t_m^3/8 - t_m^2(t - t_m)/4} \tag{1}$$

$$E_{1,2} = \frac{E_1 t - E_{1,1}(t - t_m)}{t_m} \tag{2}$$

To solve the equations above, the bending stiffness, D_{11}, membrane stiffness, E_1, and the thickness of the middle layer, t_m are needed. t_m should be chosen as large as possible to reduce the resulting stiffness for layer 2, $E_{1,2}$, but without causing negative stiffnesses for layer 1 and 3, $E_{1,1}$. For the current study the thickness of the middle layer is chosen as $t_m = 0.1 \times t$.

The binder is modelled with a mixed-mode traction separation law, see Fig. 7, using ABAQUS' built-in cohesive interface formulation.

Table 4
Model input parameters.

Material		Interface	
E_1	50 GPa	K_n	15 GPa/m
E_3	0.1 GPa	K_s	5.0 GPa/m
G_{13}	2.0 GPa	t_n^0	5.0×10^4 Pa
ν_{13}	0.0	t_s^0	1.0×10^8 Pa
D_{11}	5.0×10^{-2} N m	G_{Ic}	1.6×10^2 J/m^2
ρ	1.38×10^3 kg/m^3	G_{IIc}	1.0×10^3 J/m^2

Damage is initiated once the maximum onset traction is reached:

$$\max\left\{\frac{|t_n|}{t_n^0}, \frac{t_{s1}}{t_{s1}^0}, \frac{t_{s2}}{t_{s2}^0}\right\} \tag{3}$$

where t_n is the normal traction, t_{s1} is the transverse traction along direction 1 and t_{s2} is the transverse traction along direction 2. The superscript 0 indicates the onset traction, which is a material parameter. Once the damage is initiated, the critical energy release rate, G, is used to determine the damage evolution,

$$G = G_I + G_S \geq G_c \tag{4}$$

where G_I is the mode-I energy release rate and G_S is the shear loading mode which is the combination of the mode II and mode III energy release rate. For the quasi-2D case considered in this study, mode III is not relevant. G_c is the critical energy release rate that is interpolated between the critical energy release rate for mode-I, G_{Ic}, and mode-II, G_{IIc} using the Benzeggagh–Kenane criterion [44],

$$G_c = G_{Ic} + (G_{IIc} - G_{Ic})B^\eta, \quad B = \frac{G_S}{G_I + G_S} \tag{5}$$

where η is a power coefficient, which is a fitting parameter to experimental results. For the following model $\eta = 1$ is chosen, which gives a linear interpolation of the critical energy release rate.

The model is constrained to plane strain deformations by only modelling it with one element in the width direction and fixing all DoFs in the 2-direction (see Fig. 7). The model may be used in 3D forming problems by characterising properties in the other direction. Furthermore, the model is fixed at the left end (where the clamp is applied in the experiments), and free at the right end. The vacuum pressure is modelled as a hydrostatic pressure on the top layer of the preform. The load is applied in the course of 1.5 s to decrease the computational time of the model while still keeping inertial effects minimal. To ensure smooth forming of the preform, the load is applied in two smooth steps: the first applies $5.0 \cdot 10^3$ Pa in the course of 1.0 s and the second step increases the load to $5.0 \cdot 10^4$ Pa in the course of 0.5s. The model is kept at full pressure for 0.5 s to ensure that it is in equilibrium.

3.2. Material characterisation

The three governing material parameters for describing preform deformation and formation of wrinkles have been experimentally characterised in previous works by the authors [41,42,45]. These are the bending stiffness, D_{11}, the transverse shear stiffness, K_s, and the critical energy release rate of the bindered interface, G_{IC} (to describe binder delamination). The characterisation is carried out by a cantilever bending test [45,46] for the bending stiffness, a transverse shear test [41] for the transverse shear stiffness and a T-peel test [42] for the critical energy release rate, see Fig. 8. The resulting constant material properties are listed in Table 4. More information on the experimental characterisation can be found in the mentioned references.

Other than the characterised material properties the stiffness in the 1- and 3-direction (E_1 and E_3) are needed. Both stiffnesses potentially influence the critical time increment. E_1 is chosen as 50 GPa and E_3 is chosen as 0.1 GPa as this gives a reasonable computational time while not introducing spurious compaction. The transverse shear stiffness should be as high as possible without influencing the critical time step to avoid influencing the bending behaviour of the NCF. It is chosen as $G_{13} = 2.0$ GPa, as this value does not impact the critical time step, while limiting intra-ply shear deformation of the plies. Note that, even though intra-ply transverse shearing is expected [41] the transverse shear behaviour is modelled through the interface only to avoid it influencing the bending behaviour. Poisson effects for NCF are disregarded and the mass damping coefficient is set to 50 in the simulation. For the interface model K_n, t_n^0, t_s^0, and G_s have been fitted to the model by a parameter study, again by balancing computational time. All material properties for the model are listed in Table 4. The friction coefficient between the preform and the mould is set to 0.1.

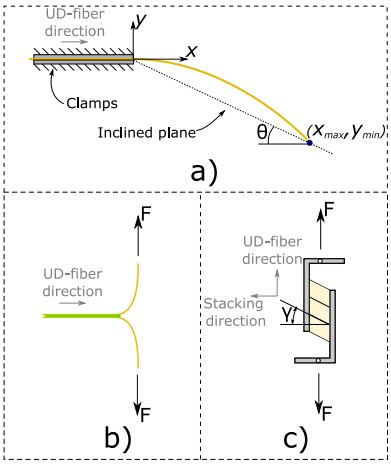

Fig. 8. Experiments carried out for characterising material properties for the model: cantilever bending test for the fabric bending stiffness (a), t-peel test for the binder toughness (b), and transverse shear stiffness for the preform transverse shear stiffness (c) [41].

3.3. Simulation results

The results from the simulation are shown in Figs. 9 and 13 for geometry 1 and 2, respectively. The wrinkle metrics and transverse shear angles for the two simulations are listed in Tables 2 and 3. In Figs. 10 and 14, the compressive strains in the preform on geometry 1 and 2, respectively, are plotted. The strains are plotted with the max value envelope, meaning that elements with a negative max value are in compression in all integration points through the thickness.

The model predicts a large mould wrinkle at the top transition and a large surface wrinkle at the bottom transition for the simulation on geometry 1. This agrees with what is observed in the experiments. The location of the simulated wrinkle at the top transition is −17 mm (relative to the transition), which is 6 mm from the wrinkles observed in the experiments. The amplitude of the simulated wrinkle is three times as large as the average amplitude measured in the experiments, while the length of the wrinkle is approximately twice as large in the simulation. The simulated wrinkle at the bottom transition is located at −2mm relative to the transition edge. This means that it is located between the max and min observed wrinkles in the experiments. The amplitude of the wrinkle is approximately twice as large as for the measured wrinkles, and the length is approximately 50% as large. From Fig. 9 it can be observed that the model predicts binder damage (delamination) at the wrinkle sites, while limited damage to the binder is predicted in the shear region. This corresponds with what is observed in the experiments where the preform after deformation has a 'hinge-like' behaviour at the wrinkle sites. This is shown in Fig. 11. The evolution of the wrinkles during loading is shown in Fig. 12. After 0.88 s the binder starts to degrade at the top transition and after 1

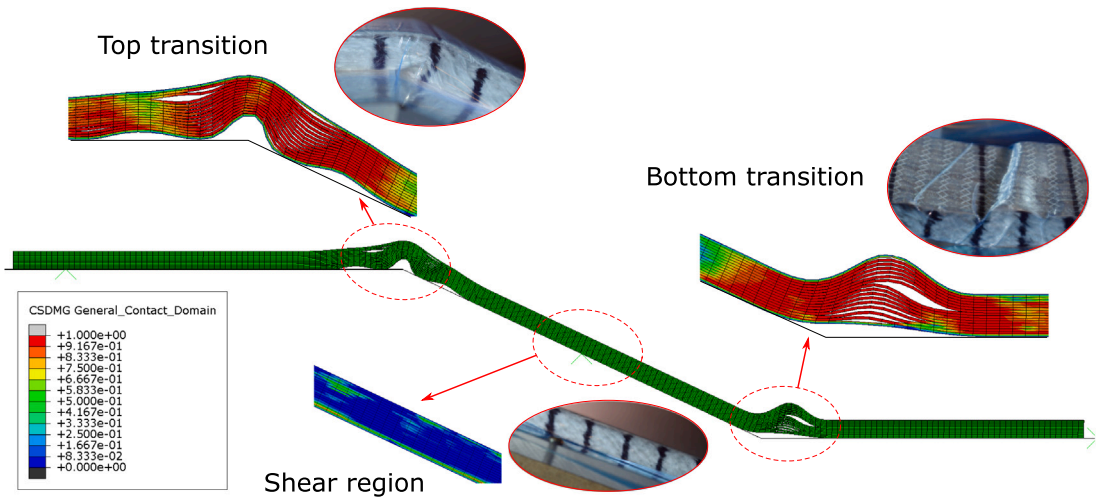

Fig. 9. Results from the simulation of the specimen being formed over geometry 1. The zoomed-in areas show interfacial damage predicted by the model, with blue areas being undamaged interfaces and red areas being fully damaged.

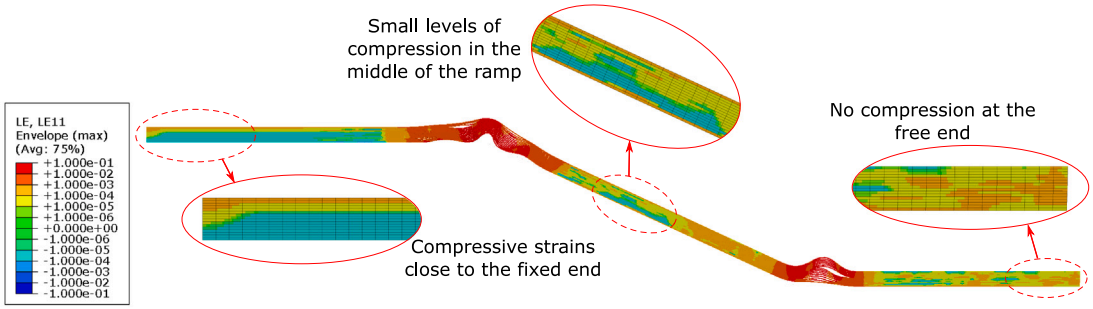

Fig. 10. Compressive strains in the preform when formed over geometry 1. The strain values are the maximum strain values in each element (max strain envelope).

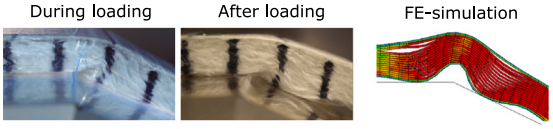

Fig. 11. Wrinkle at the top transition during loading (left), after the load is removed (centre), and in the FE-simulation (right).

s a wrinkle has formed at the transition with binder damage limited to the wrinkle site. At 1.28 s the wrinkle at the bottom transition arises, which causes the wrinkle and damage at the top transition to propagate. In Fig. 10, it is observed that there are larger compressive strains close to the fixed end than the free end where the fabric layers can slide. These compressive strains indicate an increased risk of small wrinkles appearing close to the fixed end.

For the simulation at geometry 2, the model predicts no wrinkling at the bottom transition, which corresponds well with what is observed in the experiments. As the model is made at the macro-scale, it should not be capable of predicting the small wrinkles observed in the experiments. The model, however, predicts some large wrinkling at the top transition, which is not observed in the experiments. However, based on the compressive strains in Fig. 14 there may be some small wrinkling at the top transition that cannot be captured by the camera placed inside the ramp. The model predicts that there is no damage to the binder except at the top transition. In the experiments, no hinge-like behaviour was observed after loading on geometry 2 (except for test 5), which indicates that the binder interface is intact. In test 5 however, hinge-like behaviour was observed at the top transition after unloading, which suggests that there is damage to the binder and associated ply wrinkling. This may indicate that the preform is more prone to wrinkling at the top transition as the model also predicts.

To study the influence of removing the binder material on preform forming, the simulation on benchmark geometry 1 has been carried out with a frictional law instead of a cohesive law in the fabric interface. The results show that a fabric without binder forms easily without any wrinkling. The reason for this, is that most deformation occurs before the preform contacts the tool, as seen in Fig. 12.

4. Discussion

Based on the results and observations from the experiments and simulations the wrinkle mechanisms in stabilised preforms are illustrated in Fig. 15. When the preform is loaded in bending, buckling of the rovings occurs at low loads. The experimental and numerical findings in this study suggest that roving-buckling does not cause any delamination of the binder. The rovings may buckle both out-of-plane (as sketched in Fig. 15) and in-plane [13]. As the load increases, larger wrinkles appear due to the whole NCF buckling, which is associated with damage to the binder material (delamination between plies). The damage is, thus occurring during development of the ply wrinkling.

When forming the preform over a mould with a ramp, large wrinkling occurs at the geometric transitions. As discussed in Section 2.4, this wrinkling is associated with excessive fibre length at the transitions due to a difference in transverse preform shear and ramp angle. The behaviour of the binder is expected to play a huge role in the transverse shear stiffness of the preform. To obtain wrinkle-free forming a trade-off between the ability of the binder to stabilise the NCF layers (see Fig. 15) and the increase in transverse shear stiffness (decrease in formability) is, therefore, sought. At the bottom transition (concave

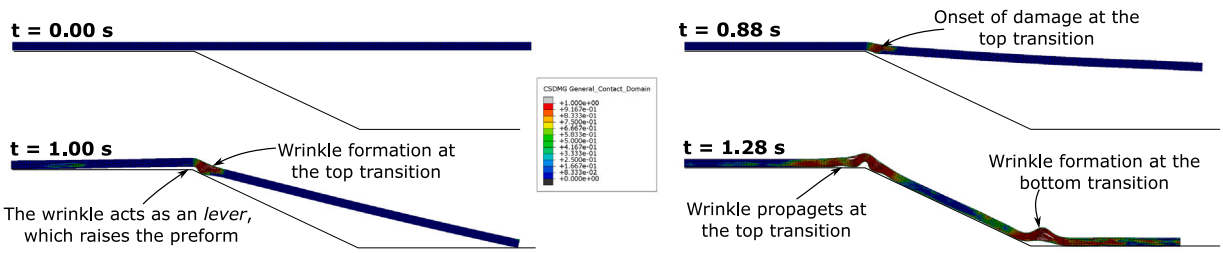

Fig. 12. Evolution of the wrinkles during loading.

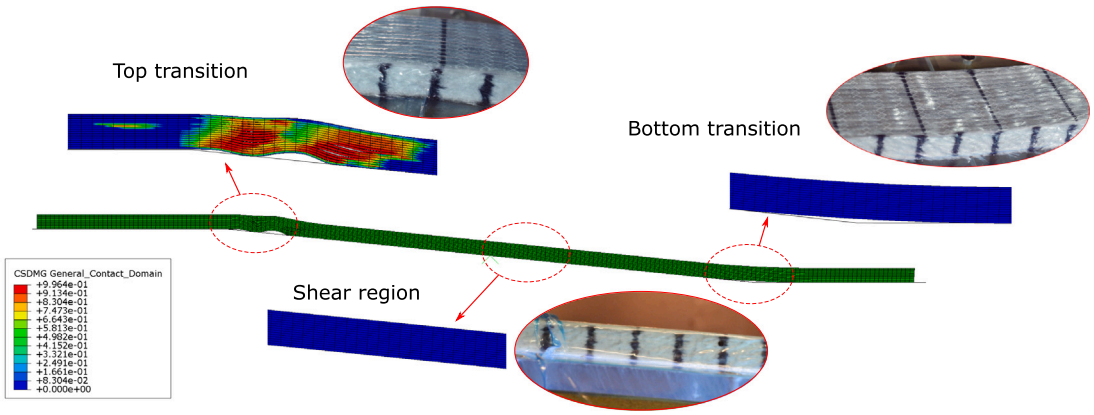

Fig. 13. Results from the simulation of the specimen being formed over geometry 2. The zoomed-in areas show interfacial damage predicted by the model, with blue areas being undamaged interfaces and red areas being fully damaged.

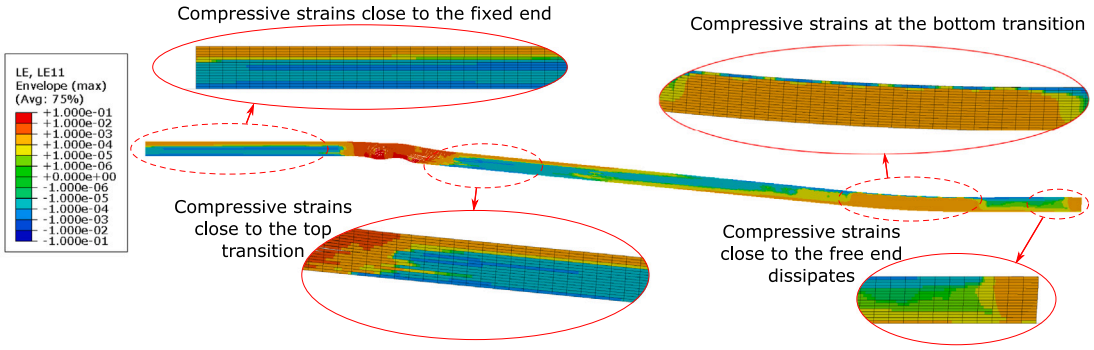

Fig. 14. Compressive strains in the preform when formed over geometry 2. The strain values are the maximum strain values in each element (max strain envelope).

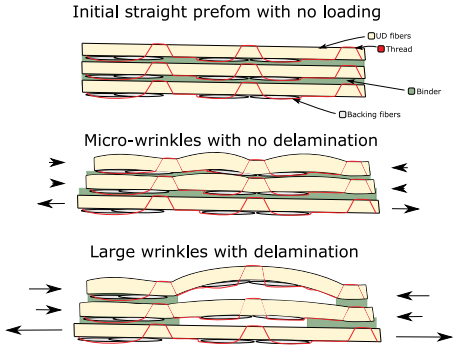

Fig. 15. Sketch of the mechanisms leading to wrinkling in the preforms.

transition) the wrinkles are facing towards the bag side, while the wrinkles at the top transition (convex transition) are facing towards the mould. The wrinkles at the top transition are, therefore, critical as they may be difficult to detect in an industrial setting. Furthermore, the results from simulating forming of the preform over geometry 2 indicated that the preform is more prone to wrinkling at the top transition. One reason for the preform being more prone to wrinkling at the top transition is that the curvature of the preform is smaller at the bottom transition due to bridging of the preform, see Fig. 16, while the preform may be more compacted at the top transition [47,48]. This will allow the excessive length of the plies to be distributed over a larger arc length at the bottom transition than at the top transition. Another explanation for the model predicting wrinkles at the top transition is that the binder is damaged at the top transition first and thus has more time to develop. The wrinkles at the top transition are, therefore, more critical for two reasons: they may be triggered more easily (due to a higher curvature) and they are not visible from the surface.

The model can be used to predict the creation of large wrinkles (wrinkling of the whole NCF), but not small wrinkles (roving-buckling) as it is a macro-scale model that assumes the NCF to behave as a homogenous continuum. Comparing the wrinkles predicted by the

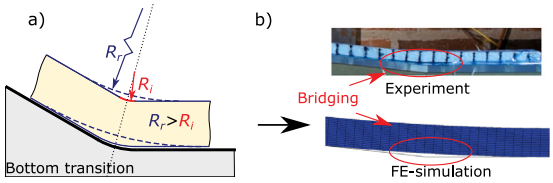

Fig. 16. (a) When the preform is formed over the bottom transition bridging may occur, which causes the real radius of curvature of the top ply (R_r) to be larger than the radius of curvature for ideal preform forming (R_i). (b) Bridging observed in the experiments and model.

model and the wrinkles observed in the experiment, the size of the wrinkles is over-predicted by the model. One reason for this is that the bending stiffness of the NCFs is modelled as constant, whereas, the UD-NCF considered in this study has a highly non-constant bending stiffness [46] with the bending stiffness decreasing at high curvatures (hinge behaviour). Another reason why the model may over-predict large wrinkles is due to its inability to capture the small meso-scale wrinkles observed in the experiments due to the macro-scale nature of the model. These small wrinkles better distribute the excess length, which will reduce the size of the larger wrinkles. A possible way to incorporate this into the model would be to increase the compliance of the material model in compression. The modelling of the vacuum bag may also contribute to different wrinkles predicted by the model. Specifically, a vacuum bag that does not conform to the mould causes membrane stresses, which may increase the pressure at convex transitions. [36]. In the model, the vacuum is modelled with a hydrostatic pressure. By modelling the vacuum bag, the pressure at the top transition may increase, which can result in smaller wrinkles predicted by the model. The friction between the bag and the top layer is not expected to influence the results as the main deformations occur due to forming, see Fig. 12, where the normal loads on the preform are small. The small wrinkles may also cause a critical knock-down in strength [10]. One way to account for them in the model is to consider the compressive strains of the NCFs. Small wrinkles may be then expected if the compressive strains are high.

5. Conclusion

This paper presents the results of an experimental campaign on wrinkles arising during forming of binder-stabilised preforms over a ramp geometry together with a new numerical preform model that can predict the creation of wrinkles. The experimental test is carried out with full-thickness preforms, consisting of 16 layers of UD-NCF stabilised with a polymeric binder, on two different ramp geometries with a ramp angle of 25.1° (steep) and 5.7° (gentle), respectively. During testing the preforms are loaded to 50% vacuum. When the load is applied, the wrinkles and transverse shear angles are measured. For the test carried out on the steep ramp geometry, large surface wrinkles are observed at the transition edge with the wrinkles at the top transition facing towards the mould and the wrinkles at the bottom transition facing towards the surface. The average transverse shear angle is measured to 7.1°, which is less than the ramp angle. On the gentle ramp geometry, small surface wrinkles are observed at the bottom transition, while the average transverse shear angle is measured to 1.9°.

The macro-scale numerical model considers the NCFs as a homogeneous continuum and the binder as a homogenous interface. To account for the micro-mechanical effects of the NCFs the bending and membrane stiffness is decoupled using a fictive 3-layer layup, while the binder interface is modelled with a mixed mode traction-separation law. The model is able to accurately predict the creation of wrinkles and is used to aid the discussion on wrinkle mechanisms during forming of the preform over the ramp geometry. For future studies on the preform model, it is recommended that material non-linearities be modelled to improve the capability of the model to accurately represent the size of the wrinkles.

Through the studies, the following wrinkle mechanisms were identified:

- Wrinkles may arise in binder-stabilised preforms when bending over geometric transitions in a mould.
- At the top transition (convex transition) the wrinkles face the mould side, while the wrinkles at the bottom transition (concave) face the bag side.
- The wrinkles are associated with excessive fabric length arising due to the difference in transverse preform shear and transition angle, which cause compression of the plies.
- For low compressive loads small wrinkles (buckling of UD-rovings) are present in the preform while the binder remains undamaged.
- For large compressive loads large wrinkles (buckling of NCF plies) arise in the preform together with damage in the binder material.
- The preform may be less prone to buckle at the bottom transition (concave) due to the bridging of the preform.

CRediT authorship contribution statement

Peter H. Broberg: Conceptualization, Methodology, Formal analysis, Investigation, Writing – original draft. **Esben Lindgaard:** Conceptualization, Methodology, Investigation, Writing – review & editing, Supervision. **Christian Krogh:** Conceptualization, Methodology, Investigation, Writing – review & editing. **Adam J. Thompson:** Methodology, Writing – review & editing. **Jonathan P.-H. Belnoue:** Methodology, Writing – review & editing. **Stephen R. Hallett:** Methodology, Writing – review & editing. **Brian L.V. Bak:** Conceptualization, Methodology, Investigation, Writing – review & editing, Supervision.

Declaration of competing interest

The authors declare that they have no known competing financial interests or personal relationships that could have appeared to influence the work reported in this paper.

Data availability

Data will be made available on request.

Acknowledgements

This study was completed as part of the MADEBLADES research project supported by the Energy Technology Development and Demonstration Program, Grant no. 64019-0514. Belnoue, Thompson and Hallett acknowledge the support of the EPSRC through the funding of the grant SIMulation of new manufacturing PROcesses for Composite Structures (SIMPROCS) (EP/P027350/1) and Composites: Made Faster (EP/V039210/1) grants.

References

[1] Zangenberg J, Brøndsted P, Koefoed M. Design of a fibrous composite preform for wind turbine rotor blades. Mater Des 2014;56:635–41. http://dx.doi.org/10.1016/j.matdes.2013.11.036.

[2] Hagenbeek M, Van Den Boom SJ, Werter NPM, Talagani F, Van Roermund M, Bulder BH, et al. The blade of the future: wind turbine blades in 2040. Tech. rep., 2022, www.tno.nl.

[3] Ohlendorf JH, Richrath M, Franke J, Brink M, Thoben KD. Towards automation of wind energy rotor blade production: a review of challenges and application examples. Adv Manuf Polym Compos Sci 2020;6(4):173–90. http://dx.doi.org/10.1080/20550340.2020.1838224.

[4] Helber F, Carosella S, Middendorf P. Effects of reactive and non-reactive tackifying agents on mechanical neat resin and composite performance for preforming processes and Liquid Resin Infusion (LRI) techniques. Adv Manuf Polym Compos Sci 2023;9(1). http://dx.doi.org/10.1080/20550340.2023.2205796, –.

[5] Fuchs ER, Field FR, Roth R, Kirchain RE. Strategic materials selection in the automobile body: Economic opportunities for polymer composite design. Compos Sci Technol 2008;68(9):1989–2002. http://dx.doi.org/10.1016/j.compscitech.2008.01.015.

[6] Nosrat Nezami F, Gereke T, Cherif C. Active forming manipulation of composite reinforcements for the suppression of forming defects. Composites A 2017;99:94–101. http://dx.doi.org/10.1016/j.compositesa.2017.04.011.

[7] Potter K, Khan B, Wisnom M, Bell T, Stevens J. Variability, fibre waviness and misalignment in the determination of the properties of composite materials and structures. Composites A 2008;39(9):1343–54. http://dx.doi.org/10.1016/j.compositesa.2008.04.016.

[8] Nelson J, Riddle T, Cairns D. Effects of defects in composite wind turbine blades – part 1: Characterization and mechanical testing. Wind Energy Sci 2017;2:641–52. http://dx.doi.org/10.5194/wes-2-641-2017.

[9] Bender J, Hallett S, Lindgaard E. Investigation of the effect of wrinkle features on wind turbine blade sub-structure strength. Compos Struct 2019;218:39–49. http://dx.doi.org/10.1016/j.compstruct.2019.03.026.

[10] Bender J, Hallett S, Lindgaard E. Parametric study of the effect of wrinkle features on the strength of a tapered wind turbine blade sub-structure. Compos Struct 2019;218:120–9. http://dx.doi.org/10.1016/j.compstruct.2019.02.065.

[11] Thor M, Sause MGR, Hinterhölzl RM. Mechanisms of origin and classification of out-of-plane fiber waviness in composite materials—a review. J Compos Sci 2020;4(3). http://dx.doi.org/10.3390/jcs4030130.

[12] Prodromou A, Chen J. On the relationship between shear angle and wrinkling of textile composite preforms. Composites A 1997;28(5):491–503. http://dx.doi.org/10.1016/S1359-835X(96)00150-9.

[13] Lee JS, Hong SJ, Yu W-R, Kang TJ. The effect of blank holder force on the stamp forming behavior of non-crimp fabric with a chain stitch. Compos Sci Technol 2007;67(3):357–66. http://dx.doi.org/10.1016/j.compscitech.2006.09.009.

[14] Boisse P, Colmars J, Hamila N, Naouar N, Steer Q. Bending and wrinkling of composite fiber preforms and prepregs. A review and new developments in the draping simulations. Composites B 2018;141:234–49. http://dx.doi.org/10.1016/j.compositesb.2017.12.061.

[15] Pandey R, Sun C. Mechanisms of wrinkle formation during the processing of composite laminates. Compos Sci Technol 1999;59(3):405–17. http://dx.doi.org/10.1016/S0266-3538(98)00080-3.

[16] Tam AS, Gutowski TG. Ply-slip during the forming of thermoplastic composite parts. J Compos Mater 1989;23(6):587–605. http://dx.doi.org/10.1177/002199838902300604.

[17] Dodwell T, Butler R, Hunt G. Out-of-plane ply wrinkling defects during consolidation over an external radius. Compos Sci Technol 2014;105:151–9. http://dx.doi.org/10.1016/j.compscitech.2014.10.007.

[18] Farnand K, Zobeiry N, Poursartip A, Fernlund G. Micro-level mechanisms of fiber waviness and wrinkling during hot drape forming of unidirectional prepreg composites. Composites A 2017;103:168–77. http://dx.doi.org/10.1016/j.compositesa.2017.10.008.

[19] Guzman-Maldonado E, Wang P, Hamila N, Boisse P. Experimental and numerical analysis of wrinkling during forming of multi-layered textile composites. Compos Struct 2019;208:213–23. http://dx.doi.org/10.1016/j.compstruct.2018.10.018.

[20] Huang J, Boisse P, Hamila N, Zhu Y. Simulation of wrinkling during bending of composite reinforcement laminates. Materials 2020;13(10). http://dx.doi.org/10.3390/ma13102374.

[21] Hallander P, Akermo M, Mattei C, Petersson M, Nyman T. An experimental study of mechanisms behind wrinkle development during forming of composite laminates. Composites A 2013;50:54–64. http://dx.doi.org/10.1016/j.compositesa.2013.03.013.

[22] h. Shih C, Liu Q, Lee QLJ. Vacuum-assisted resin transfer molding using tackified fiber preforms. Polym Compos 2001;22(6):721–9.

[23] Allaoui S, Cellard C, Hivet G. Composites : Part a effect of inter-ply sliding on the quality of multilayer interlock dry fabric preforms. Composites A 2015;68:336–45. http://dx.doi.org/10.1016/j.compositesa.2014.10.017.

[24] Krogh C, Bak BLV, Lindgaard E, Olesen AM, Hermansen SM, Broberg PH, et al. A simple MATLAB draping code for fiber-reinforced composites with application to optimization of manufacturing process parameters. 2021, p. 457–71.

[25] Bussetta P, Correia N. Numerical forming of continuous fibre reinforced composite material: A review. Composites A 2018;113(July):12–31. http://dx.doi.org/10.1016/j.compositesa.2018.07.010.

[26] Dangora LM, Mitchell CJ, Sherwood JA. Predictive model for the detection of out-of-plane defects formed during textile-composite manufacture. Composites A 2015;78:102–12. http://dx.doi.org/10.1016/j.compositesa.2015.07.011.

[27] Dörr D, Schirmaier FJ, Henning F, Kärger L. A viscoelastic approach for modeling bending behavior in finite element forming simulation of continuously fiber reinforced composites. Composites A 2017;94:113–23. http://dx.doi.org/10.1016/j.compositesa.2016.11.027.

[28] Thompson AJ, Belnoue JP-H, Hallett SR. Modelling defect formation in textiles during the double diaphragm forming process. Composites B 2020;202:108357. http://dx.doi.org/10.1016/j.compositesb.2020.108357.

[29] Döbrich O, Gereke T, Diestel O, Krzywinski S, Cherif C. Decoupling the bending behavior and the membrane properties of finite shell elements for a correct description of the mechanical behavior of textiles with a laminate formulation. J Ind Text 2014;44(1):70–84. http://dx.doi.org/10.1177/1528083713477442.

[30] Yu F, Chen S, Harper LT, Warrior NA. Simulating the effect of fabric bending stiffness on the wrinkling behaviour of biaxial fabrics during preforming. Composites A 2021;143(2020). http://dx.doi.org/10.1016/j.compositesa.2021.106308.

[31] Erland S, Dodwell T, Butler R. Characterisation of inter-ply shear in uncured carbon fibre prepreg. Composites A 2015;77:210–8. http://dx.doi.org/10.1016/j.compositesa.2015.07.008.

[32] Vanclooster K, Lomov S, Verpoest I. Simulation of multi-layered composites forming. Int J Mater Form 2010;3:695–8. http://dx.doi.org/10.1007/s12289-010-0865-2.

[33] Dörr D, Joppich T, Kugele D, Henning F, Kärger L. A coupled thermomechanical approach for finite element forming simulation of continuously fiber-reinforced semi-crystalline thermoplastics. Composites A 2019;125(July):105508. http://dx.doi.org/10.1016/j.compositesa.2019.105508.

[34] Wang Y, Mahapatra S, Belnoue JP, Ivanov DS, Hallett SR. Understanding tack behaviour during prepreg-based composites' processing. Composites A 2023;164(2022):107284. http://dx.doi.org/10.1016/j.compositesa.2022.107284.

[35] Belnoue J, Nixon-Pearson O, Thompson A, Ivanov D, Potter K, Hallett S. Consolidation-driven defect generation in thick composite parts. J Manuf Sci Eng 2018;140. http://dx.doi.org/10.1115/1.4039555.

[36] Thompson AJ, McFarlane JR, Belnoue JP, Hallett SR. Numerical modelling of compaction induced defects in thick 2D textile composites. Mater Des 2020;196:109088. http://dx.doi.org/10.1016/j.matdes.2020.109088.

[37] Rashidi A, Belnoue JP, Thompson AJ, Hallett SR, Milani AS. Consolidation-driven wrinkling in carbon/epoxy woven fabric prepregs: An experimental and numerical study. Composites A 2021;143(January):106298. http://dx.doi.org/10.1016/j.compositesa.2021.106298.

[38] Beex L, Peerlings R. An experimental and computational study of laminated paperboard creasing and folding. Int J Solids Struct 2009;46(24):4192–207. http://dx.doi.org/10.1016/j.ijsolstr.2009.08.012.

[39] Charmetant A, Orliac J, Vidal-Sallé E, Boisse P. Hyperelastic model for large deformation analyses of 3d interlock composite preforms. Compos Sci Technol 2012;72(12):1352–60. http://dx.doi.org/10.1016/j.compscitech.2012.05.006.

[40] Jimenez Martin C, Maes VK, McMahon T, Kratz J. Influence of NCF architecture on the morphology of forming induced wrinkling. Front Mater 2023;10(February):1–11. http://dx.doi.org/10.3389/fmats.2023.1126933.

[41] Broberg PH, Shakibapour F, Jakobsen J, Lindgaard E, Bak BLV. Characterisation of the transverse shear behaviour of binder-stabilised preforms for wind turbine blade manufacturing. Compos Struct 2024;328:117738. http://dx.doi.org/10.1016/j.compstruct.2023.117738.

[42] Broberg PH, Krogh C, Lindgaard E, Bak BLV. Simulation of wrinkling during forming of binder stabilized UD-NCF preforms in wind turbine blade manufacturing. Key Eng Mater 2022;926:1248–56. http://dx.doi.org/10.4028/p-165q46.

[43] Broberg PH, Krogh C, Lindgaard E, Bak BLV. Predicting fibre wrinkling in binder-stabilised preforms during wind turbine blade manufacturing. In: Vassilopoulos A, Michaud V, editors. In: Proceedings of the 20th European conference on composite materials - composites meet sustainability, vol. E, EPFL Lausanne, Composite Construction Laboratory; 2022, p. 224–31. http://dx.doi.org/10.5075/epfl-298799_978-2-9701614-0-0, eCCM20 - The 20th European Conference on Composite Materials ; Conference date: 26-06-2022 Through 30-06-2022.

[44] Benzeggagh ML, Kenane M. Measurement of mixed-mode delamination fracture toughness of unidirectional glass/epoxy composites with mixed-mode bending apparatus. Compos Sci Technol 1996;56:439–49.

[45] Broberg PH, Lindgaard E, Krogh C, Jensen SM, Trabal GG, Thai AF, Bak BLV. One-click bending stiffness: Robust and reliable automatic calculation of moment–curvature relation in a cantilever bending test. Composites B 2023;260(2022). http://dx.doi.org/10.1016/j.compositesb.2023.110763.

[46] Krogh C, Broberg PH, Kepler J, Jakobsen J. Comprehending the bending: A comparison of different test setups for measuring the out-of-plane flexural rigidity of a UD fabric. Key Eng Mater 2022;926:1257–67. http://dx.doi.org/10.4028/p-r883x4.

[47] Hubert P, Poursartip A. Aspects of the compaction of composite angle laminates: an experimental investigation. J Compos Mater 2001;35(1):2–26. http://dx.doi.org/10.1106/X8D7-PR9V-U6F2-0JEK.

[48] Levy A, Hubert P. Vacuum-bagged composite laminate forming processes: Predicting thickness deviation in complex shapes. Composites A 2019;126(August):105568. http://dx.doi.org/10.1016/j.compositesa.2019.105568.